JOURNAL OF AIRCRAFT
Vol. 33, No. 4, July–August 1996

Adaptive Flutter Suppression of an Unswept Wing

Indranil Danda Roy* and Walter Eversman†
University of Missouri–Rolla, Rolla, Missouri 65401

The purpose of this study was to investigate the potential of an adaptive feedforward controller for active flutter suppression of a flexible wing. The flexible wing structure was modeled by a multi-degree-of-freedom finite element representation with beam elements for bending and rod elements for torsion. Control action was provided by a flap attached to the trailing edge of the wing, but extending for only a short length along the wingspan. The dynamics of the entire structure were simulated using only the first few flexible modes, thereby resulting in a reduced-order system for time integration. Both quasisteady and unsteady aerodynamics were used to generate the airforces acting on the wing. An adaptive feedforward controller was designed based on the filtered-X least mean squares (LMS) algorithm. The control configuration included an on-line system identification that provided the LMS controller with a reasonably accurate model of the plant. The linear wing model in closed loop exhibited highly damped responses at airspeeds where the open-loop responses were destructive. Simulations with the flexible wing model in a time-varying airstream showed a 36% increase over the open-loop flutter airspeed. With 10% measurement noise introduced in the model, it demonstrated good robustness to the extraneous disturbances. Since the controller structure was adaptive, its effectiveness was not limited by the form of aerodynamics used in this investigation to model the airforces. In the example studied it was found that adaptation was rapid enough to successfully control flutter at accelerations in the airstream of up to 7 ft/s^2.

Introduction

THE last two and a half decades have seen successful research take place in the field of active flutter suppression. Researchers have employed various control methodologies to develop flutter control schemes.

Nissim[1] developed active flutter control laws based on the concept of aerodynamic energy. According to his theory, for all stable oscillatory motions of an elastic system in an airstream, positive work must be done by the system on the surrounding medium. However, his concept was only useful for simple aeroelastic models. Horikawa and Dowell[2] explained the wing flutter suppression problem with simple active feedback controls using a standard root–locus technique. The objective was to obtain insight into the control of converging frequency flutter such as the classical bending–torsion flutter of a wing.

Modern control design methods in state space seem more compatible with general multi-input/multi-output (MIMO) systems and many techniques such as the linear quadratic optimal control theory (LQ), linear quadratic Gaussian (LQG) methodology, and eigenstructure assignment have been used.[3,4] Active flutter suppression laws based on LQG design and order reduction, classical design like root locus and Nyquist techniques, and other concepts have been developed at the NASA Langley Research Center, and they have been implemented and successfully tested on an aeroelastically scaled wind-tunnel model in the NASA Langley Transonic Dynamic Tunnel.[5] These modern control techniques, though robust, when applied to active flutter suppression may suffer from the fact that the states of the model are greatly augmented to recast the aerodynamic frequency response matrices into state space. These added states are fictitious, unobservable, and very sensitive to the modeling approximations.

Received Dec. 10, 1994; revision received Dec. 28, 1995; accepted for publication Feb. 14, 1996.

*Graduate Research Assistant, Department of Mechanical and Aerospace Engineering and Engineering Mechanics.

†Curators' Professor, Department of Mechanical and Aerospace Engineering and Engineering Mechanics. Associate Fellow AIAA.

Instances of adaptive control techniques used to design flutter suppression laws are relatively few in the literature. Research performed jointly at the MIT Laboratory for Information and Decision Systems and Honeywell Systems and Research Center was successful in applying the adaptive control concept of the self-tuning regulator (STR) to suppress wing/store flutter instabilities.[6] Adaptive signal processing was enhanced in the 1970s with the development of the least mean square (LMS) algorithm.[7,8] Widrow et al.[9,10] developed an adaptive control scheme where the controller was placed in cascade with the plant and its parameters were continually updated by the LMS algorithm to minimize a certain performance criterion. Since the controller was fed with a filtered version of the excitation signal, rather than the signal itself, it became known as the filtered-X LMS algorithm. Elliott et al.[11] extended the single-channel filtered-X LMS concept and designed a multichannel (or multiple error) feedforward LMS controller. They also discussed the application of this algorithm to active sound and vibration control where the LMS controller was used to drive secondary sources to reduce the levels of noise or vibrational fields by minimizing the sum of squares of a number of error sensor signals. This multichannel LMS controller was observed to be very robust to errors involved in modeling of the plant. Boucher et al.[12] showed that the single-channel filtered-X LMS controller, in the case of slow adaptation, converged even when the phase error associated with the plant model was as high as 90 deg. The controller was virtually unaffected when the phase error associated with the plant model was 45 deg or less. Sommerfeldt and Tichy[13] investigated the problem of minimizing the force transmitted through a two-stage vibration isolation mount. The controller was implemented in real time and demonstrated 30- to 40-dB attenuation of the transmitted vibration for periodic excitations.

The adaptive scheme introduced here is of the feedforward type and generates a secondary disturbance using control actuators to cancel out the primary disturbance created by the source excitation. Since the control algorithm is adaptive in nature, it is not necessary to have an accurate a priori knowledge of the plant to be controlled. For a given system and a performance index, the adaptive scheme finds a way of identifying the unknown plant and providing effective control.

Also, the adaptive controller is capable of tracking changing system parameters in case the plant happens to be time-varying. The wing structure in a time-varying airstream is necessarily a plant with changing parameters. In addition, complex aeroelastic structures can sometimes be difficult to model accurately. Therefore, a filtered-X LMS based adaptive controller with an on-line system identification process would be very suitable for active flutter suppression.

Finite Element Model of the Wing

A finite element representation has been used to develop the dynamic structural model of the flexible wing. The flexible wing structure is approximated by a cantilevered beam with a c.m. offset from its neutral axis. Along with Euler–Bernoulli bending, the flexible model also incorporates torsion. Therefore, a beam/rod finite element model of the structure is developed that acts like a beam in bending and a rod in torsion. The finite element mesh is constructed of Hermitian beam C^2 elements and Lagrangian rod C^1 elements. As previously mentioned, the elastic axis is chosen to be the neutral axis of the beam so that the bending and torsion of the straight wing structure are structurally uncoupled statically. The top diagram in Fig. 1 shows a finite element mesh for a representative wing model consisting of six elements. Each beam/rod element has six degrees of freedom; three degrees of freedom at each node. These include one translational degree of freedom, the bending displacement $u1$ and $u2$, and two rotational degrees of freedom that describe the bending slope $u3$ and $u4$ and the torsional motion about the elastic axis $u5$ and $u6$, respectively.

To account for the variation of airforces along the span of the wing, aerodynamic strip theory has been utilized. According to this theory, the airforces at any spanwise station on the wing are related to the angle of attack and/or control flap deflection only at that location. To implement the strip theory the aerodynamic wing model has been discretized into several panels. The bottom diagram in Fig. 1 shows a representative wing model consisting of six aerodynamic panels with a finite element node at the center of each panel. This ensures full compatibility of the aerodynamic model with the finite element structural model shown in Fig. 1. Note that although Fig. 1 shows six elements (panels), numerical simulations presented here have been performed with nine elements (panels). Each panel has the provision of having a rigid flap at its trailing edge. If a panel has a control flap, then an additional discrete degree of freedom representing the control flap rotation is associated with the panel.

The element stiffness matrix is constructed following the standard finite element method. The element mass matrix is formed using a lumped approach where the mass properties of each panel are lumped at its center of mass. The motion of each panel is defined by the finite element node located at the elastic axis. Upon assembly of the element mass and stiffness matrices, the equations of motion for free vibration of the entire structure can be written as

$$\begin{bmatrix} [M_{ee}] & [M_{ec}] \\ [M_{ce}] & [M_{cc}] \end{bmatrix} \begin{bmatrix} \ddot{w}_e \\ \ddot{w}_c \end{bmatrix} + \begin{bmatrix} [K_{ee}] & [K_{ec}] \\ [K_{ce}] & [K_{cc}] \end{bmatrix} \begin{bmatrix} w_e \\ w_c \end{bmatrix} = 0 \quad (1)$$

where the global mass and stiffness matrices have been partitioned according to the elastic (constraint-fixed) degrees of freedom w_e and the constraint degrees of freedom w_c. Note that both w_e and w_c include the bending displacements, bending

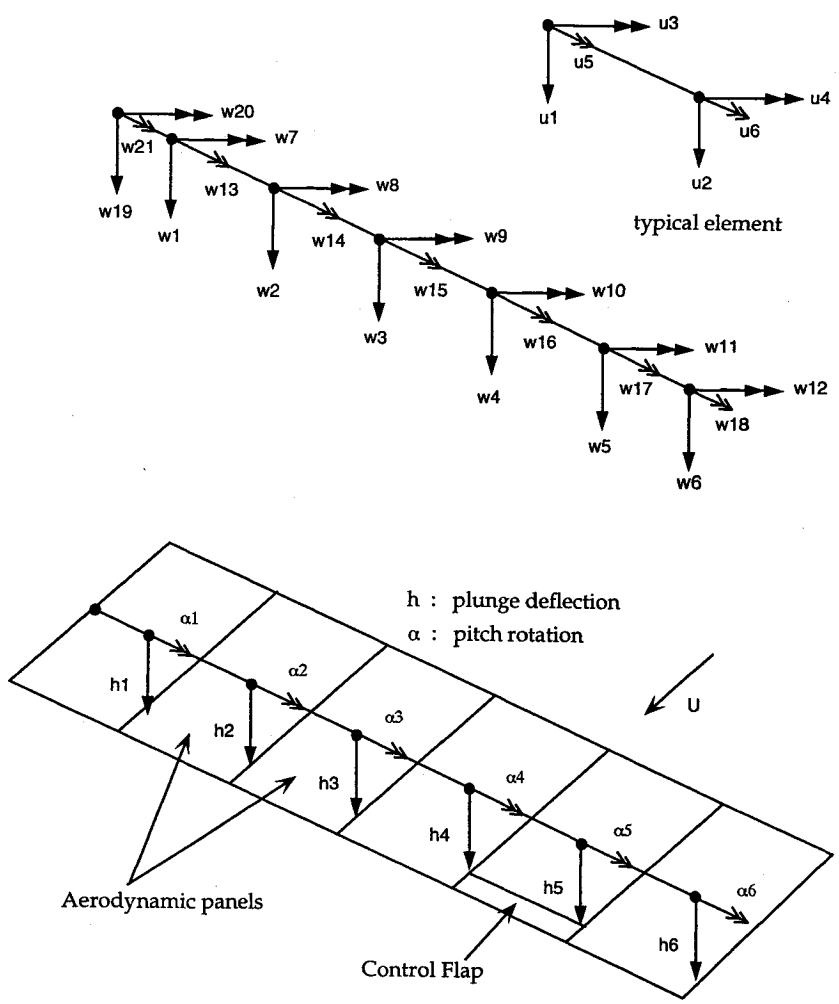

Fig. 1 Structural and aerodynamic models of the flexible wing.

slope, torsional and control flap rotation degrees of freedom. Since the root of the flexible wing is fixed in this study $w_c = 0$, and the constraint–fixed elastic motions are defined by

$$[M_{ee}]\ddot{w}_e + [K_{ee}]w_e = 0 \tag{2}$$

A standard eigenanalysis of Eq. (2) yields n natural frequencies, $w_1, \ldots, w_n$, and their corresponding eigenvectors ϕ_i, $i = 1, \ldots, n$, n, being the number of elastic degrees of freedom. Since the first few elastic modes are sufficient to describe the dynamical motion of the flexible wing structure, the first m ($m < n$) eigenvectors are retained to form the modal matrix:

$$[\phi] = [\phi_1\ \phi_2 \cdots \phi_m] \tag{3}$$

Numerical simulations have been performed on two wing models that have the same structural model but different aerodynamic models. Quasisteady two-dimensional aerodynamics represent the air forces on one model while time domain unsteady aerodynamics are used for the other. The purpose of this is to demonstrate that the performance of the adaptive LMS controller is not restricted by the aerodynamic models studied in this investigation.

Two-dimensional quasisteady aerodynamics, which include damping because of plunge, represent the aerodynamic lift L, aerodynamic moment M_{ac}, and the hinge moment M_h for each panel as

$$L = qScC_{l\alpha}[\alpha + (\dot{h}/U)] + qScC_{l\delta}\delta \tag{4}$$

$$M_{ac} = qSc^2C_{m\delta}\delta \tag{5}$$

$$M_h = qSc_h^2C_{h\alpha}\alpha + qSc_h^2C_{h\delta}\delta \tag{6}$$

where U is the airspeed, q is the dynamic pressure, S is the span of the panel, c is the total chord, c_h is the chord of the control flap, h is the plunge displacement, α is the pitch rotation, δ is the control flap deflection, and $C_{l\alpha}$, $C_{l\delta}$, $C_{m\delta}$, $C_{h\alpha}$, and $C_{h\delta}$ are the appropriate aerodynamic coefficients. The approximate values of these aerodynamic coefficients and other geometric and structural parameters used in the simulations have been provided in Table 1. Lift is positive upward and aerodynamic moment on the airfoil is positive leading-edge up. To account in an approximate way for the finite span effects, a correction factor (parabolic drop from wing root to tip) has been applied to the aerodynamic coefficients shown in Table 1.

Using Eqs. (4–6), the global aerodynamic damping matrix $[C_a]$, the global aerodynamic stiffness matrix $[K_a]$, and the global load vector F_c are constructed by forming the generalized forces corresponding to the global degrees of freedom. Note that this form of aerodynamic representation ignores the bending slope degrees of freedom.

Augmentation of the aerodynamic damping matrix, aerodynamic stiffness matrix, and the load vector to the system equations of motion yields

$$[M_{ee}]\ddot{w}_e + [C_a]\dot{w}_e + ([K_{ee}] + [K_a])w_e = F_c\delta_c \tag{7}$$

where δ_c is the command control rotation input to the flap. Since the first few flexible modes define the wing model dynamics, numerical integration of the equations of motion have been carried out in the reduced-order modal domain. Using the truncated modal matrix $[\phi]$, modal transformation of the system equations (7) yield

$$[M^*]\ddot{y} + ([C^*] + [C_s])\dot{y} + [K^*]y = F^*\delta_c \tag{8}$$

where $[M^*]$, $[C^*]$, and $[K^*]$ are the generalized mass, damping, and stiffness matrices, respectively. In this investigation $[C_s]$ represents an additional structural modal damping matrix that introduces a 2% viscous damping in all of the retained modes.

To introduce simple unsteady aerodynamics, the lift L and the total moment M acting on each panel can be written as

$$\dot{L} + \beta_1(U/b)L = qScC_{l\alpha}\{(1 - a_1)\dot{W} + \beta_1(U/b)W\} + qScC_{l\delta}\{(1 - a_1)\dot{\delta} + \beta_1(U/b)\delta\} \tag{9}$$

$$\dot{M} + \beta_1(U/b)M = qScC_{l\alpha}b(\tfrac{1}{2} + a)\{(1 - a_1)\dot{W} + \beta_1(U/b)W\} + qSc^2C_{m\delta}\{(1 - a_1)\dot{\delta} + \beta_1(U/b)\delta\} \tag{10}$$

where b is the semichord, ab is the location of the elastic axis aft of the midchord, a_1 and β_1 are aerodynamic parameters ($a_1 = 0.5$ and $\beta_1 = 0.05$), and W is defined by

$$W(t) = (\dot{h}/U) + \alpha + (\tfrac{1}{2} - a)(b/U)\dot{\alpha} \tag{11}$$

This is consistent with a first-order lag model as an approximation to the Wagner function.[14]

The equations of motion of the wing in the physical space can now be written as

$$[M_{ee}]\ddot{w}_e + [C_s]\dot{w}_e + [K_{ee}]w_e = F_c\delta_c + Q(t) \tag{12}$$

where $Q(t)$ is the vector of generalized aerodynamic forces and can be defined by the first-order differential equation in vector matrix form

$$\dot{Q} + \beta_1(U/b)Q = [A]\ddot{w}_e + [B]\dot{w}_e + [C]w_e \tag{13}$$

$[A]$, $[B]$, and $[C]$ are the aerodynamic matrices resulting from

Table 1 Geometric, structural, and aerodynamic parameters of the wing model

Variable	Description	Value
S	Span of wing	24.5 in.
c	Chord	7.0 in.
c_h/c	Ratio of flap chord to total chord	0.25
EI	Elastic modulus	2×10^4 lbf-in.^{2}
GJ	Shear modulus	1×10^3 lbf-in.^{2}
m	Mass/length	2.24×10^{-4} lbf-s^2/in.^{2}
i	Torsional moment of inertia/length	4.79×10^{-4} lbf-s^2/in.
x_c	Distance of elastic axis from leading edge	1.75 in.
x_p	Distance of c.m. from leading edge	2.2 in.
$C_{l\alpha}$	Lift coefficient/angle of attack	2π
$C_{l\delta}$	Lift coefficient/flap deflection	4.0
$C_{m\delta}$	Moment coefficient/flap deflection	−0.75
$C_{h\alpha}$, $C_{h\delta}$	Hinge moment coefficients	−0.01

Eqs. (9) and (10) for every panel. Modal transformation of Eqs. (12) and (13) using the retained modal matrix $[\phi]$ leads to

$$[M^*]\ddot{y} + [C_s^*]\dot{y} + [K^*]y = F^*\delta_c + R(t) \tag{14}$$

$$\dot{R} + \beta_1(U/b)R = [A^*]\ddot{y} + [B^*]\dot{y} + [C^*]y \tag{15}$$

where $R = \phi^T Q$ and $[A^*]$, $[B^*]$, and $[C^*]$ are modal transformations of matrices $[A]$, $[B]$, and $[C]$, respectively.

Using a standard state variable approach ($v = \dot{y}$), Eqs. (14) and (15) can be expressed as set of first-order differential equations in vector matrix form

$$\begin{Bmatrix} \dot{y} \\ \cdots \\ \dot{v} \\ \cdots \\ \dot{R} \end{Bmatrix} = \begin{bmatrix} 0 & I & 0 \\ -[M^*]^{-1}[K^*] & -[M^*]^{-1}[C_s^*] & [M]^{-1} \\ [C^*] - [A^*][M^*]^{-1}[K^*] & [B^*] - [A^*][M^*]^{-1}[C_s^*] & [A][M]^{-1} - \beta_1(U/b)I \end{bmatrix} \begin{Bmatrix} y \\ \cdots \\ v \\ \cdots \\ R \end{Bmatrix} + \begin{Bmatrix} 0 \\ \cdots \\ [M]^{-1}F^* \\ \cdots \\ [A^*][M]^{-1}F^* \end{Bmatrix} \delta_c \tag{16}$$

Equations of motion (8) and (16) in the modal domain are then solved using the fourth-order Runge–Kutta time integration scheme. The first seven flexible modes have been retained to accurately depict the dynamic behavior of the wing structure (frequency of the seventh mode is 89.84 Hz). The time step of integration (and the sampling period of the digital controller) is maintained at 0.001 s to satisfy the Nyquist sampling criteria and to account for the spread of natural frequencies in the time integration. The wing model with quasisteady aerodynamics shows a critical flutter speed of 87 ft/s at a flutter frequency of 12.69 Hz, whereas the wing model with unsteady aerodynamics predicts a critical flutter speed of 125 ft/s at a frequency of 11.72 Hz. This discrepancy is consistent with the difference in the two aerodynamic models. Both models show the predominance of the first cantilevered bending mode and the first torsional mode in flutter motions. The input from the adaptive controller to the flap is a command control rotation δ_c to the torque tube, which acts as a hinge torsional spring connecting the main body of the wing to the flap. The hinge spring is made stiff (uncoupled frequency in δ is chosen to be 60 Hz) so that the response of the open-loop system is relatively unaffected by the motion of the flap.

Adaptive Feedforward Control Scheme

The adaptive feedforward control structure is based on the filtered-X LMS algorithm developed by Widrow et al.[9,10] The elegance of the adaptive scheme presented here lies in the fact that no a priori knowledge of the plant to be controlled is necessary for successful operation of the controller. This particular feature gives it a distinct advantage over conventional feedback-type control schemes. The feedforward control structure includes an on-line adaptive system identification scheme. This provides the controller with a reasonably accurate model of the plant during the operation of the controller. Since the plant is time-varying and an off-line system identification is not practical for wing flutter suppression, this adaptive controller structure based on the filtered-X LMS algorithm seems well suited for this application.

The system identification configuration that has been used is known as the LMS output error approach. A block diagram of the adaptive identification procedure is shown in Fig. 2. A finite impulse response (FIR) digital filter is placed in parallel with the plant to be modeled. An FIR digital filter is an all-zero structure with its pulse transfer function represented as $H(z) = \sum_{i=0}^{N-1} w_i z^{-i}$, where the weights w_i represent the impulse response of the filter. Both the plant and the adaptive model are excited by the same reference command input x_k, where k is the time index. The output error of this configuration is

$$\varepsilon_k = d_k - y_k \tag{17}$$

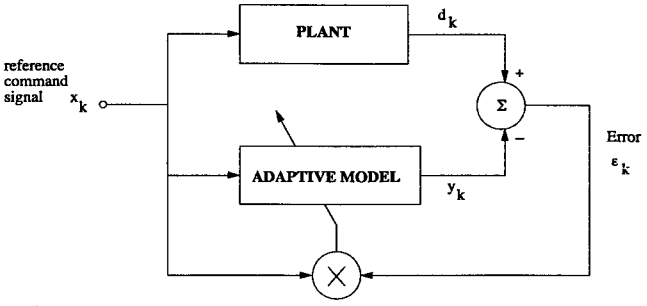

Fig. 2 System identification using LMS approach.

where d_k is the desired output of the plant and y_k is the output of the adaptive FIR filter. The weights W of the digital filter are adapted so that the mean-squared output error

$$\zeta = E[\varepsilon_k^2] \tag{18}$$

is minimized. Here the operator E denotes expectation. The weights of the FIR digital filter are continuously updated by a steepest descent approach as governed by the LMS algorithm.[7,8] The LMS algorithm approximates the gradient of the mean squared error ζ by the gradient of the instantaneous squared error ε_k^2, thereby eliminating the need of time averaging the squared error signal. This leads to the weight update equation

$$W_{k+1} = W_k + 2\mu\varepsilon_k X_k \tag{19}$$

where μ is the gain constant regulating the speed and stability of adaptation and X_k is the reference input vector. If the reference command input is persistently exciting, the weights of the adaptive filter, upon convergence, should match the impulse response of the plant very closely.

A typical block diagram of a single-channel filtered-X LMS[9,10] control structure is shown in Fig. 3. The adaptive controller is placed in cascade with the plant such that both the plant and the controller are excited with the same reference command input x_k. The plant output denoted as the error signal ε_k is the combination of the plant responses because of the disturbance input x_k and the controller output u_k, respectively. It can be written as

$$\varepsilon_k = d_k + y_k \tag{20}$$

where d_k is the primary disturbance (desired signal that needs to be canceled) and y_k is the control disturbance resulting from the control action u_k.

If the transfer function from the controller output u_k to the error signal ε_k (known as error plant or secondary plant) is represented by $H_{err}(z)$, then

$$\varepsilon(z) = d(z) + H_{err}(z)u(z) \tag{21}$$

Since the primary disturbance d_k is assumed to be correlated to the disturbance input x_k, then

$$d(z) = H_p(z)x(z) \tag{22}$$

where $H_p(z)$ is the transfer function of the primary plant that can be represented by an FIR digital filter. Substituting Eq. (22) in Eq. (21) we obtain

$$\varepsilon(z) = H_p(z)x(z) + H_{err}(z)u(z) \tag{23}$$

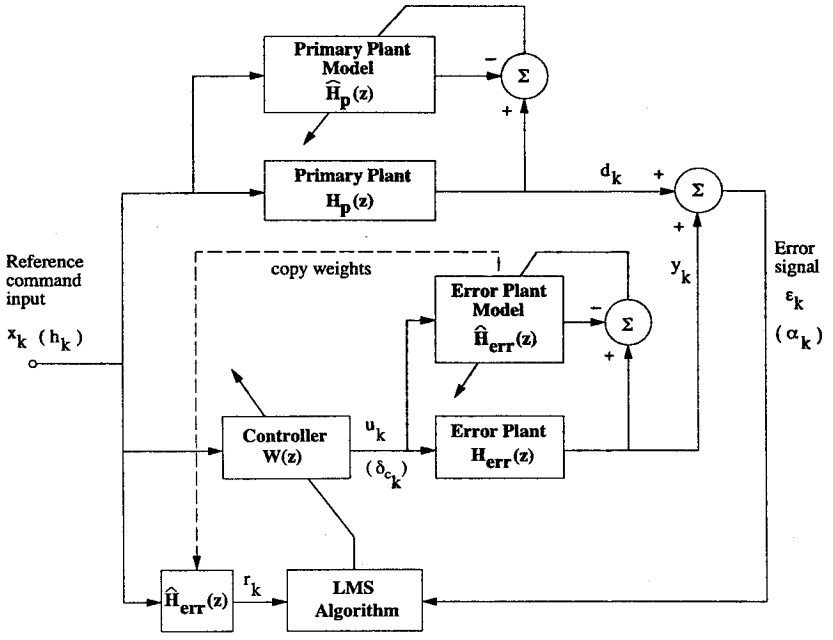

Fig. 3 Filtered-X LMS control configuration.

Since the signals x_k, u_k, and ε_k are available for measurement, an on-line adaptive system identification can be carried out to model the error plant and primary plant transfer functions simultaneously. For the on-line identification of the error plant H_{err}, the training signals that are necessary are u_k and the control disturbance y_k. For the estimation of the primary plant H_p, the appropriate signals are the reference signal x_k and the desired signal d_k. Now d_k and y_k are not independently measurable, but their sum, the error signal ε_k is. However, both the primary and the error plants are modeled by linear FIR digital filters. Expressing the plant outputs as the discrete convolution of the filter impulse responses and the corresponding input sequences yield

$$d_k = \sum_{i=0}^{I-1} \bar{h}_{p_i} x_{k-i} \tag{24}$$

$$y_k = \sum_{i=0}^{J-1} \bar{h}_{\mathrm{err}_i} u_{k-i} \tag{25}$$

where $\bar{h}_p$ and $\bar{h}_{err}$ are the impulse responses of the primary plant model and the error plant model, respectively, and I and J are the number of taps in their respective FIR filter representations. The error signal can be estimated as

$$\bar{\varepsilon}_k = \sum_{i=0}^{I-1} \bar{h}_{p_i} x_{k-i} + \sum_{i=0}^{J-1} \bar{h}_{\mathrm{err}_i} u_{k-i} \tag{26}$$

where $\bar{\varepsilon}_k$ is the estimate of the error signal found by the two filter models. If the input sequences to the two filter models and their impulse responses are expressed in vector form as

$$\boldsymbol{X}^T = [x_k x_{k_1} \cdots x_{k-I+1} u_k u_{k_1} \cdots u_{k-J+1}] \tag{27}$$

$$\bar{\boldsymbol{H}}_p^T = [\bar{h}_{p_0} \bar{h}_{p_1} \cdots \bar{h}_{p_{I-1}}] \tag{28a}$$

$$\bar{\boldsymbol{H}}_{\mathrm{err}}^T = [\bar{h}_{\mathrm{err}_0} \bar{h}_{\mathrm{err}_1} \cdots \bar{h}_{\mathrm{err}_{J-1}}] \tag{28b}$$

$$\bar{\boldsymbol{H}}^T = [\bar{\boldsymbol{H}}_p^T \bar{\boldsymbol{H}}_{\mathrm{err}}^T] \tag{28c}$$

then Eq. (26) leads to

$$\bar{\boldsymbol{E}} = \bar{\boldsymbol{H}}^T \boldsymbol{X} \tag{29}$$

where $\bar{\boldsymbol{E}}$ is the estimate of the error signal sequence in vector form.

Using the adaptive FIR filter model $\bar{\boldsymbol{H}}$ represented by Eq. (28c), the on-line system identification of the primary plant and the error plant can be carried out concurrently using the LMS approach without explicit knowledge of the signals d_k and y_k.

The adaptive controller is an FIR filter whose all-zero transfer function is given by $W(z)$. Equation (23) can be written as

$$\varepsilon(z) = H_p(z)x(z) + H_{\mathrm{err}}(z)W(z)x(z) \tag{30}$$

The LMS algorithm adapts the weights w_i ($i = 0, 1, \ldots, N-1$) of the Nth-order LMS control filter to minimize a quadratic performance index of the plant response:

$$J = E[\varepsilon_k^2] \tag{31}$$

The LMS algorithm approximates the gradient of the cost function J by the gradient of the instantaneous squared error ε_k^2. Therefore, the weight update equation of the LMS controller is of the steepest descent type given by

$$\boldsymbol{W}_{k+1} = \boldsymbol{W}_k - \gamma \varepsilon_k \boldsymbol{r}_k \tag{32}$$

where γ is the adaptive gain constant of the control filter, and

$$r(z) = \hat{H}_{\mathrm{err}}(z)x(z) \tag{33}$$

Here $\hat{H}_{err}(z)$ is the transfer function model of the error plant resulting from the on-line system identification (refer to Fig. 3). The reference input signal filtered by the error plant model is r_k (also known as the filtered-X signal). The filtered-X LMS algorithm uses this signal to update the control filter weights instead of the reference input signal x_k as in conventional LMS algorithm. To understand this, it has to be realized that the aim of this algorithm is to set up the controller in a configuration where the LMS algorithm can be readily applied to adapt its weights. From Fig. 3 it is obvious that ε_k is at the error plant output, not at the adaptive control filter output. If ε_k and x_k are

used directly with the LMS algorithm for the control filter, the adaptive process is almost guaranteed to be unstable, or if not, to find an irrelevant solution. However, it is assumed that time variations of the impulse responses of both $H_{err}(z)$ and $W(z)$ take place with time constants long compared to the combined time constants of the control filter and the error plant. Thus, with relatively slow adaptation, $W(z)$ may be considered linear and commutable with $H_{err}(z)$. If the error plant is commuted with the control filter, Eq. (30) can be modified as

$$\varepsilon(z) = H_p(z)x(z) + W(z)H_{err}(z)x(z) \tag{34}$$

or

$$\varepsilon(z) = H_p(z)x(z) + W(z)r(z) \tag{35}$$

where $r(z)$ is given by Eq. (33). Note that $\hat{H}_{err}(z)$ is used in Eq. (33) because the actual $H_{err}(z)$ is unknown. The error ε_k now appears at the adaptive control filter output. The signal x_k, however, gets filtered through the error plant model before reaching the control filter, thereby generating r_k.

Though the primary plant model $\hat{H}_p(z)$ does not have any contribution in the weight update Eq. (32), system identification of the primary plant is necessary to obtain the desired model $\hat{H}_{err}(z)$. This is because the system identification of the primary and error plants are concurrent events and one cannot take place without the other [refer to Eq. (23)]. It is apparent at this point that the system identification, though on-line, must precede the adaptive control process.

To summarize, the general properties[15] of the filtered-X LMS based control scheme are as follows:

1) It can converge on a time scale comparable with the delay in the error plant, and so can track changes in the reference signal quite rapidly.

2) Since the adaptive system identification is on-line, the scheme can track any variations in the plant while the controller is operating, provided the variations are not too rapid. Though the filtered-X LMS concept is based on slow adaptation, the algorithm has achieved successful convergence in many cases with rapid adaptation.

3) It is quite robust to errors in the estimate of the error plant transfer function used to generate the filtered reference signal.

4) It is relatively easy and inexpensive to implement as a real-time controller since high-speed digital signal processors are now more readily available than before.

For the self-excited vibrations of the wing model, there is no external disturbing force that is physically measurable. Therefore, for the flexible wing model, the reference command input x_k is chosen to be the bending (plunge) displacement h_k of the finite element node of a panel along the wingspan. The plant output to be minimized (or the error signal ε_k) is chosen to be the torsional (pitch) angle α_k of the same position. The output of the LMS controller is the command control rotation of the control flap δ_{c_k} (refer to Fig. 3) attached to the same aerodynamic panel. Since the pitch and the plunge motions of the wing are highly coupled, it is assumed that minimizing one would suppress the other. The on-line system identification process fits a digital filter $\hat{H}_p$ between the plunge and the pitch displacements of the panel and another digital filter $\hat{H}_{err}$ between the command control deflection and the pitch displacement. It provides models for the primary plant transfer function and error plant transfer function, respectively. Besides the control flap dynamics, no other external actuator dynamics have been included in the simulation model. In a real-time implementation of the controller, the choice of an appropriate actuator is not unique. However, since the system identification is on-line, the actuator dynamics could easily be adaptively modeled in the error path as long as the actuator transfer function is capable of being approximated by a linear system.

Simulation Results

The wing vibration at the onset of flutter is nearly harmonic in nature. The spectral character of the plunge and the pitch disturbance signals, measured at any location on the wing, at and beyond flutter, are narrow band and alike (i.e., the dominant peaks in both the pitch and plunge disturbance signals correspond to the same frequencies). This is true for both the aerodynamic models used for the simulations. These features make the filtered-X LMS algorithm very well suited to the problem of wing flutter suppression. First, adaptation, in both system identification and control, is fast when dealing with predominantly harmonic signals. In fact, the filtered-X LMS algorithm has been shown to yield excellent results in harmonic control.[11,13] Second, the filtered-X LMS algorithm assumes that the primary disturbance signal d_k is correlated to the reference command input signal h_k, so that appropriate cancellation at all existing frequencies is possible by creating a control disturbance y_k (Fig. 3). Therefore, we would hope to see encouraging results with the adaptive controller.

The objective of the single input/single output (SISO) adaptive control configuration is to control the flexible modes present in the motion of the structure using a single flap at the trailing edge of the aerodynamic panel whose motion is being sensed. Driving a control flap located on a panel based on the sensed information of another panel usually leads to unwanted disturbances (not necessarily unstable) in the closed-loop motion. Therefore this controller structure does not allow the use of multiple control flaps driven by a single sensor for flutter suppression. An effort has been made to optimize the location of the control flap along the span of the wing. Because of finite span effect corrections, the aerodynamic lift and moment generated from control flap deflection drop along the span from the wing root to the tip. It is observed that a single flap on the outermost panel does not produce enough control authority to suppress the rapidly divergent flutter motions. As the flap is moved towards the root, control authority increases. The simulation results discussed here pertain to a wing model made of nine aerodynamic panels with a control flap on one of the panels. For identification purposes, the panels are numbered 1–9 from the wing root to the tip. An 11% span flap, consistent with the FEM discretization (nine aerodynamic panels of equal width with a control flap on one of them), does not have sufficient authority and requires larger flap rotations to stabilize the fluttering wing. To circumvent this problem of lack of adequate authority, a control flap has been placed on the seventh panel whose width is made twice that of the other panels (resulting in a 20% span flap). This configuration allows simulation of the wing model with a larger flap (spanwise), thereby providing an increased control authority.

The response of the wing with quasisteady aerodynamics is initially simulated with the airspeed accelerating continuously from 85 to 120 ft/s (3% below critical flutter speed to 36% above), at a linear rate of 1 ft/s^2. Such a case is indicative of a mild acceleration through the flutter boundary. The wing model in this numerical test is excited by perturbing the control flap with a triangular pulse every 5 s to initiate the flutter motion. The sole purpose of this excitation is to simulate the effect of turbulence that may be in the airstream, and not to provide the training signals for error plant estimation. The on-line system identification scheme converges to a solution based on those signals that are naturally available from the wing model. Figure 4 shows the open-loop response of the wing. At subcritical flutter speeds, the wing shows damped decaying oscillations when excited. As the airspeed reaches critical flutter speed (87 ft/s) at 2 s the oscillations grow divergent, ultimately leading to structural failure. Figure 5 shows the closed-loop response of the wing structure with the controller on at all times. The system identification/controller structure adapts as the wing starts to diverge at flutter speed, but stabilizes it quickly once the adaptive process converges. Excellent flutter suppression is observed until 110 ft/s. Beyond 110 ft/s the

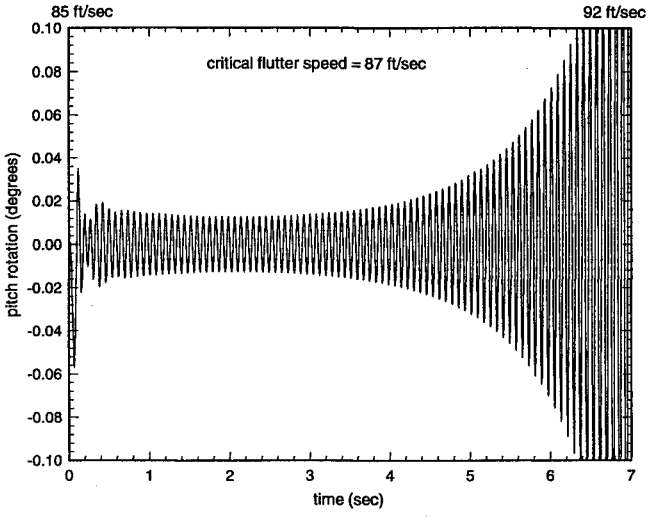

Fig. 4 Open-loop response of the wing with airspeed varying at 1 ft/s^2.

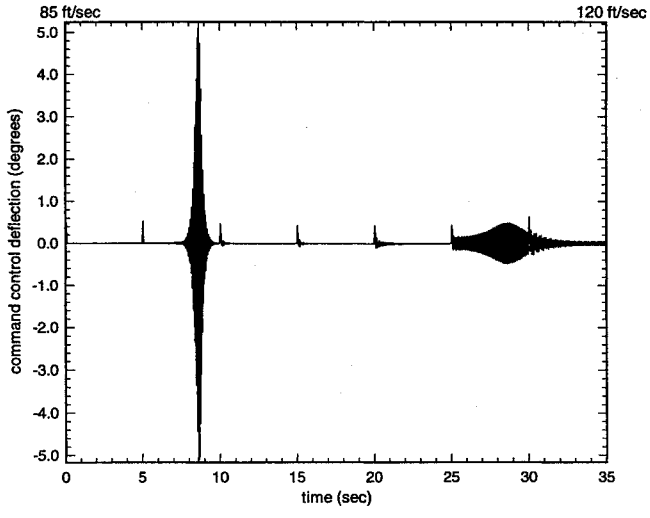

Fig. 6 Time history of the controller output (airstream acceleration at 1 ft/s^2).

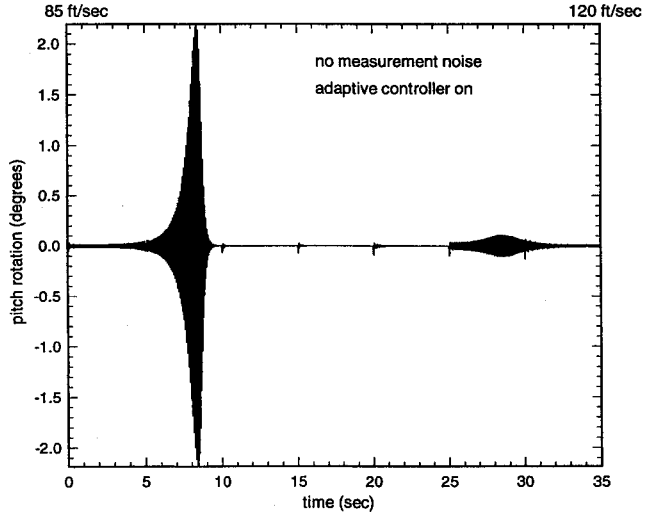

Fig. 5 Closed-loop response of the wing with airspeed varying at 1 ft/s^2.

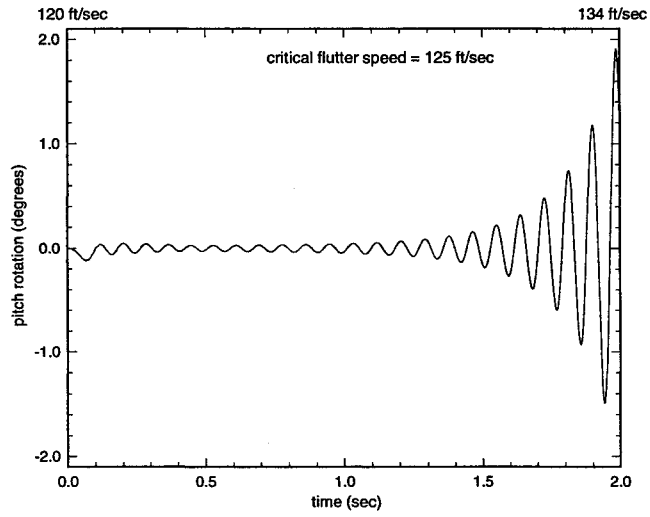

Fig. 7 Open-loop response of the wing with airspeed varying at 7 ft/s^2.

adaptive process is slow to react to the destabilizing aerodynamic forces. However, the controller is still effective until 120 ft/s (36% above flutter), beyond which the motion of the wing diverges slowly, even with the controller on. Figure 6 shows the time history of the controller output. The adaptive controller hardly affects the wing motion before it starts diverging at flutter since the adaptive process does not gain enough impetus until the sensed motions become reasonably large. The LMS controller used is a 32nd-order FIR digital filter.

Numerical simulations are then performed with the wing model with unsteady aerodynamics. The airspeed is varied continuously from 120 to 170 ft/s (4% below critical flutter speed to 36% above) at a rate of 7 ft/s^2. This is indicative of a more rapid acceleration through the flutter boundary. The control flap is perturbed every 3 s to initiate the flutter motion. Figure 7 shows the open-loop response of the wing, whereas Fig. 8 illustrates the closed-loop response of the wing structure with the controller on at all times. The controller, in this case, is able to suppress the flutter up to an airspeed 36% above open-loop flutter speed. The LMS controller reacts to this model in a way very similar to the wing model with quasi-steady aerodynamics that was discussed earlier. Since the system identification/controller structure is completely adaptive, the phasing relations between control flap rotation, structural deformation, and generation of airforces defined by unsteady aerodynamics have been suitably incorporated in the primary and the error plant models. Figure 9 portrays the time history of the controller output. Again, the controller is not effective until the flutter motion becomes significant. It then acts rapidly to stabilize the system. Figure 10 depicts the convergence process of the adaptive LMS control filter. The filter weights remain virtually unaffected until the onset of flutter, where they undergo a sharp rise in their values, indicating quick and forceful control action to suppress the rapidly divergent motions of the wing. The number of taps used in the FIR digital control filter is 50.

To investigate the effect of sensor noise on the performance of the adaptive controller, numerical simulations have been performed (on the wing model with unsteady aerodynamics) with 10% uncorrelated measurement noise introduced individually at the sensed plunge displacement and pitch rotation signals (other parameters are identical to the case without noise). The noise is determined from a random sample following a Gaussian probability distribution[16] with mean $\mu_m = 0$ and standard deviation $\sigma = 0.1A_{max}$, where A_{max} is the maximum amplitude of the signal for the case with no noise introduced in the sensors. Figure 11 shows the closed-loop response of the wing structure with noisy reference and error signals fed to the adaptive controller. It clearly demonstrates the inherent robustness of the adaptive control scheme to unaccounted noise

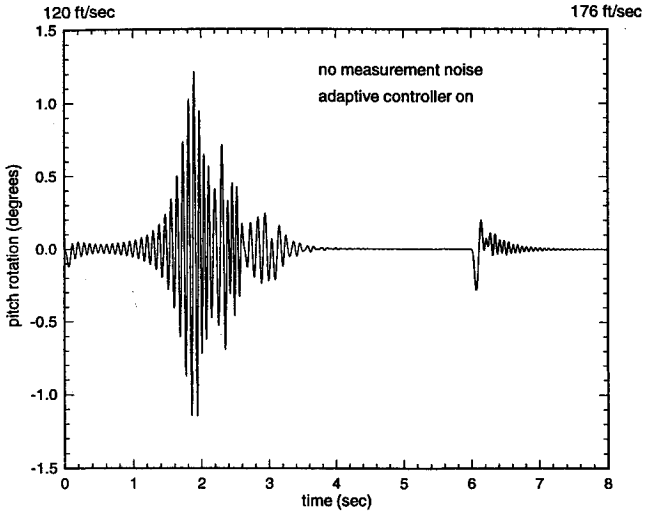

Fig. 8 Closed-loop response of the wing with airspeed varying at 7 ft/s^2.

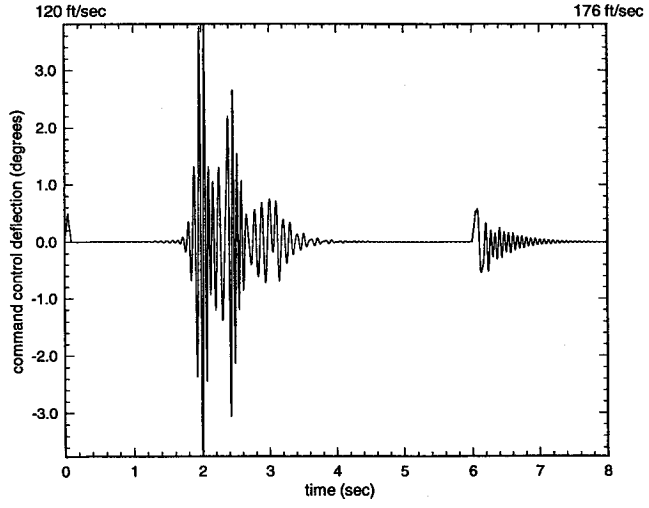

Fig. 9 Time history of the command control input (airspeed acceleration is 7 ft/s^2).

in the system. Figures 12 and 13 portray the time history of the noisy controller output and the convergence of its controller filter weights, respectively. The deviation of these time histories from the case without noise is not very significant. From Fig. 13 it is apparent that the measurement noise contributes to noise in the weights of the adaptive control filter. In this case, the value of the mean squared error that the LMS control filter minimizes does not go to zero after convergence is achieved. Instead, it randomly varies about a mean value close to zero, where the mean value is dependent on signal-to-noise ratio of the measured signals. The measurement noise therefore is uncontrolled, and appears in time histories of the system parameters only as an additive element.

The adaptive LMS controller has performed satisfactorily in suppressing flutter of the wing without any prior knowledge of the model. However, the performance of this SISO control configuration is limited by the acceleration of the airstream (i.e., the rate at which the plant varies). As the acceleration is increased beyond 7 ft/s^2, the controller is unable to adapt rapidly enough to successfully suppress the instability. This failure can be attributed to two related factors. First, the single control flap lacks the control authority to suppress the rapidly diverging motion of the wing. Second, because of rapid acceleration, the controller does not have enough time to adapt before the system diverges. A MIMO configuration of the adaptive LMS

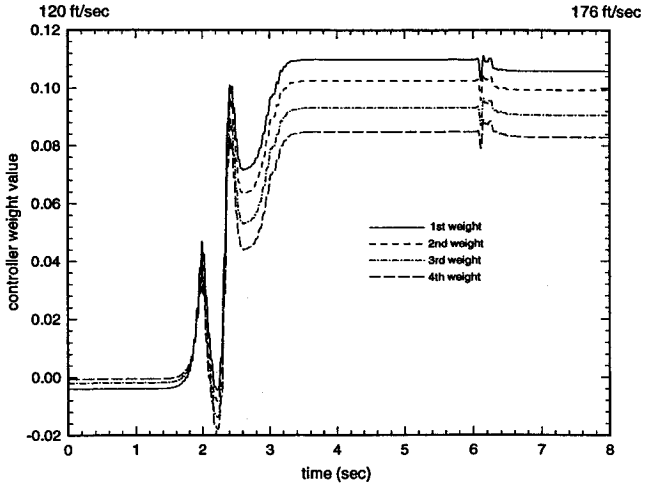

Fig. 10 Convergence of the first four controller weights (airstream acceleration 7 ft/s^2).

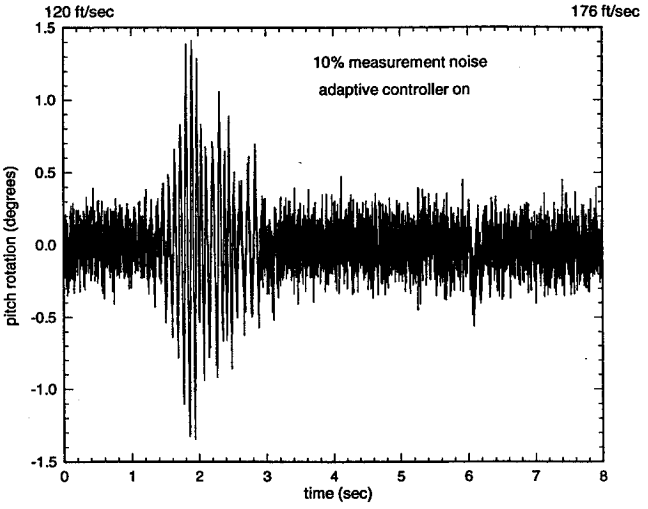

Fig. 11 Closed-loop response of the wing with airstream varying at 7 ft/s^2 (with sensor noise).

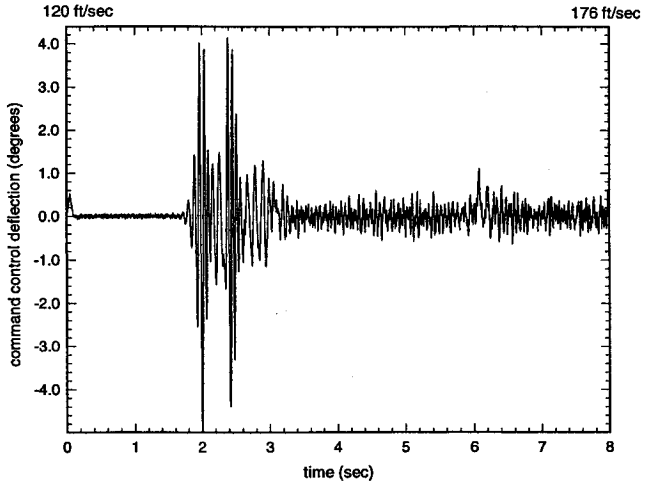

Fig. 12 Time history of the noisy controller output.

controller would allow the use of more than one flap resulting in an increased control authority. However, this form of an adaptive control configuration (SISO or MIMO) is always going to be limited by an acceleration threshold beyond which it would lack the speed of adaptation to cope with the destabilizing system.

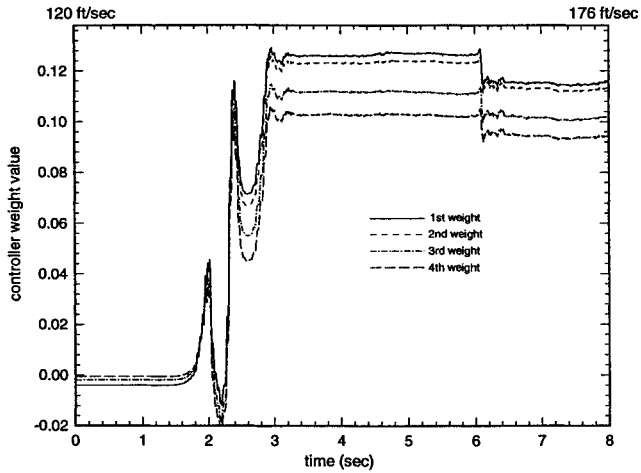

Fig. 13 Time history of the first four weights of the noisy LMS controller.

Summary

The main objective of this study was to ascertain the feasibility of using an adaptive feedforward control structure for active flutter suppression of a flexible wing. For numerical simulation purposes, a multi-degree-of-freedom finite element structural model of a flexible wing was constructed. The control actuator for this model was a flap attached to the trailing edge of the wing and extending along 20% of the wingspan. An adaptive feedforward controller was developed based on the filtered-X LMS algorithm originally introduced by Widrow et al.[9,10] The controller structure included an on-line system identification scheme that provided the LMS controller with a reasonably accurate model of the plant. In numerical simulations, the effectiveness of the controller acting on the wing structure was evaluated with the airspeed varying from a subcritical flutter speed to 36% above the critical flutter speed. The adaptive controller with its on-line system identification scheme was able to track the changing plant parameters and showed excellent suppression of the divergent wing motions above flutter. Since the controller structure was adaptive, its performance was not affected by the aerodynamics used in this study to model the air forces. The control scheme also was demonstrated to be very robust to measurement noise. However, the SISO control configuration failed to provide flutter suppression during very rapid accelerations of the airstream (above 7 ft/s^2) because of insufficient control authority and the inability of the adaptive process to cope with such rapid changes. A MIMO control configuration may extend the envelope of successful adaptation and should be investigated.

Acknowledgment

The authors would like to thank William Tranter of the Electrical Engineering Department at the University of Missouri–Rolla for his valuable assistance in the adaptive filter theory.

References

[1]Nissim, E., "Flutter Suppression Using Active Control Based on the Concept of Aerodynamic Energy," NASA TN-D-6199, March 1971.

[2]Horikawa, H., and Dowell, E. H., "An Elementary Explanation of the Flutter Mechanism with Active Feedback Controls," *Journal of Aircraft*, Vol. 16, No. 4, 1979, pp. 225–232.

[3]Mahesh, J. K., Stone, C. R., Garrard, W. L., and Dunn, H. J., "Control Law Synthesis for Flutter Suppression Using Linear Quadratic Gaussian Theory," *Journal of Guidance and Control*, Vol. 4, No. 4, 1981, pp. 415–422.

[4]Garrard, W. L., and Liebst, B. S., "Active Flutter Suppression Using Eigenspace and Linear Quadratic Design Techniques," *Journal of Guidance, Control, and Dynamics*, Vol. 8, No. 3, 1985, pp. 304–311.

[5]Perry, B., Mukhopadhayay, V., Hoadley, S., Houck, J., Buttrill, C., and Cole, S., "Digital Flutter Suppression System Investigations for the Active Flexible Wing Wind-Tunnel Model," *Proceedings of the AIAA/ASME/ASCE/AHS/ASC 31st Structures, Structural Dynamics, and Materials Conference* (Long Beach, CA), AIAA, Washington, DC, 1990, pp. 1571–1581.

[6]Johnson, T. L., Harvey, C. A., and Stein, G. N., "Self-Tuning Regulator Design for Adaptive Control of Aircraft Wing/Store Flutter," Lab. for Information and Decision Systems, Massachusetts Inst. of Technology, Cambridge, MA, Dec. 1980.

[7]Widrow, B., "Adaptive Filters," *Aspects of Network and System Theory*, edited by R. E. Kalman and N. De Claris, Holt, Rinehart, and Winston, Philadelphia, PA, 1970, pp. 563–587.

[8]Widrow, B., Glover, J. R., Jr., McCool, J. M., Kaunitz, J., Williams, S., Hearn, R. J., Zeidler, J. R., Dong, E., Jr., and Goodlin, R. C., "Adaptive Noise Cancelling: Principles and Applications," *Proceedings of the IEEE*, Vol. 63, No. 12, 1975, pp. 1692–1716.

[9]Widrow, B., Shur, D., and Shaffer, S., "On Adaptive Inverse Control," *Proceedings of the ASILOMAR 15th ASILOMAR Conference on Circuits, Systems, and Computers* (Pacific Grove, CA), U.S. Naval Postgraduate School, Univ. of Santa Clara, and IEEE, 1981, pp. 185–195.

[10]Widrow, B., and Stearns, S. D., *Adaptive Signal Processing*, Prentice–Hall, Englewood Cliffs, NJ, 1985.

[11]Elliott, S. J., Stothers, I. M., and Nelson, P. A., "A Multiple Error LMS Algorithm and Its Application to the Active Control of Sound and Vibration," *IEEE Transactions on Acoustics, Speech and Signal Processing*, Vol. ASSP-35, No. 10, 1987, pp. 1423–1434.

[12]Boucher, C. C., Elliott, S. J., and Nelson, P. A., "Effect of Errors in the Plant Model on the Performance of Algorithms for Adaptive Feedforward Control," Special Issue on Adaptive Filters: Theory and Practice, *IEE Proceedings-F*, Vol. 138, No. 4, 1991, pp. 313–319.

[13]Sommerfeldt, S. D., and Tichy, J., "Adaptive Control of a Two-Stage Vibration Isolation Mount," *Journal of the Acoustical Society of America*, Vol. 88, No. 2, 1990, pp. 938–944.

[14]Bislinghoff, L. J., Ashley, H., and Halfman, R. L., *Aeroelasticity*, Addison–Wesley, Reading, MA, 1955.

[15]Nelson, P. A., and Elliott, S. J., *Active Control of Sound*, Academic, London, 1992.

[16]Bain, L. J., and Engelhardt, M., *Introduction to Probability and Mathematical Statistics*, PWS-KENT Publishing Co., Boston, MA, 1992.